

Coherent Integration Time: The Longer, the Better

A common assumption in GNSS receiver design is that the coherent integration time should be less than a few dozens of milliseconds. This makes perfect sense for today's commercial receivers due to data bit transitions, oscillator jitter, and user dynamics. However, a coherent integration time of several seconds would mitigate three important indoor positioning problems: multipath, cross-correlation false locks, and the squaring loss. Extending the integration time has a price, typically requiring an assistance data link providing data bits (or the use of pilot signals), a stable oscillator, and a sophisticated GNSS/INS integration to compensate for non-linear user motion. This column describes how those issues have been solved and the resulting benefits as demonstrated by a recently built prototype with a sensitivity of around 1.5 dBHz, more than 10 decibels beyond the current state of the art.



THOMAS PANY, BERNHARD RIEDL, JÓN WINKEL
IFEN GMBH

THOMAS WÖRZ, ROBERT SCHWEIKERT
AUDENS ACT CONSULTING GMBH

HERBERT NIEDERMEIER
UNIVERSITY FAF MUNICH

STEFANO LAGRASTA
TELESPAZIO S.P.A

GUSTAVO LÓPEZ-RISUEÑO
DAVID JIMÉNEZ-BAÑOS
ESA/ESTEC

The European Space Agency (ESA) funded the development of a new GNSS/INS navigation system called DINGPOS to assess the potential utility of Galileo signals and current (L1) and new (L5) GPS signals for indoor positioning. The DINGPOS project also investigated new indoor positioning methods for pedestrians based on those signals and other sensors.

The integrated system may have applications as a pedestrian navigation system (PNS) for emergency forces and in the military domain. A key feature of the new system is its support of a coherent integration over several seconds of GNSS signal processing and the fusion of a multitude of positioning sensors.

The system incorporates an L1/L5 GNSS software receiver, a microelectromechanical inertial measurement unit (MEMS IMU) including a magnetometer and a barometer, WiFi power readings, as well as a ZigBee-based radio navigation system. **Figure 1** shows a prototype of the system integrated onto a backpack.

A software receiver acts as the integration platform, decoding the GNSS signals at E1=L1 and E5a=L5 and synchronizing the IMU, magnetometer, barometer, WiFi, and ZigBee data with the GNSS intermediate frequency (IF) samples. The IMU synchronization accuracy is +/- 2 microseconds.

Data processing can be done in real-time or in postprocessing. The software

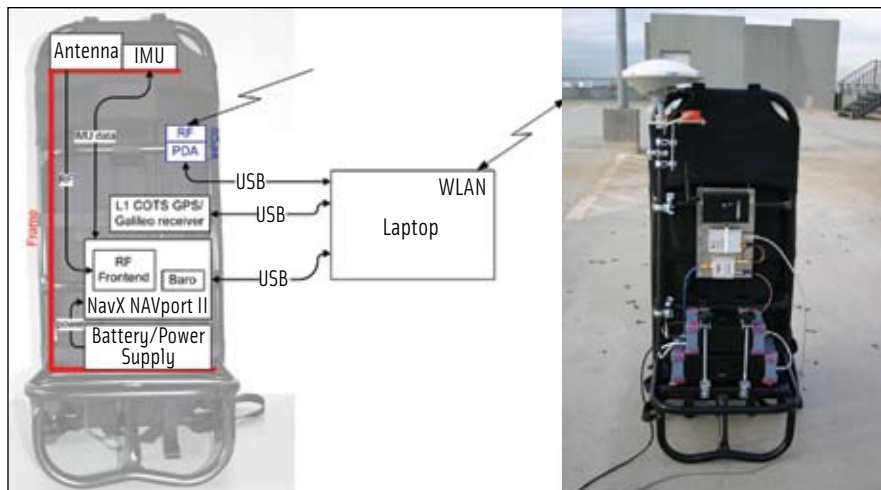


FIGURE 1 Mounting of the DINGPOS receiver

receiver provides an application programming interface (API) and manages the data-flow for this GNSS/INS integration. DINGPOS specific C/C++ code was developed to realize ultra-high sensitivity signal processing and integrated positioning (Figure 5). The algorithms are loaded into the software receiver as dynamic link libraries (DLLs). A second software receiver acts as a reference station to provide assistance data (including navigation message data bits), coarse start position, and time synchronization via the network time protocol.

The prototype is an ultra-tightly coupled (UTC — sometimes also called deeply coupled) GNSS/IMU system. This integration method — patented many years ago — is an excellent way to optimally combine the short-term stability of the IMU data with the long-term stability of the GNSS measurements. Many research publications have described integrated GNSS/INS systems and methods.

The core elements of this method are a strapdown calculation for IMU data processing and an error state Kalman filter using GNSS observations. The strapdown algorithm computes a user trajectory (after a coarse/fine alignment procedure) and the Kalman filter estimates the error of this trajectory with respect to the true trajectory. The filter fully controls the GNSS correlation process by providing numerically controlled oscillator (NCO) rate and phase values for code and carrier tracking.

By linking all GNSS channels via the Kalman filter, *vector tracking* is realized. Vector tracking may come in several flavors depending on the observations used and the Kalman state vector as summarized in a work by J.-H. Won et alia cited in the Additional Resources section near the end of this article.

UTC can be realized in a non-coherent and in a coherent way. A non-coherent system uses Doppler and code pseudoranges as observations and neglects the carrier phase. Its positioning accuracy is at the meter level, but it can track extremely low power GNSS signals. The article by D. Landis et alia listed in Additional Resources describes a nice prototype implementation of non-coherent integration.

A coherent system makes use of the GNSS carrier phase and must be able to predict the carrier phase from its internal states. Consequently, the (relative) positioning accuracy is at the millimeter to centimeter level; however, such systems generally have a reduced sensitivity compared to the non-coherent approach. Further details of this

approach can be found in the article by M. Petovello et alia.

For the envisaged DINGPOS prototype we wanted to use a MEMS IMU so as to achieve a low bill of materials. However, this IMU technology has an insufficient gyro bias stability required to realize a coherent UTC system, especially in an indoor environment with very inaccurate GNSS updates. Therefore, the strapdown approach was abandoned, and the IMU data was used in a different way.

The new approach allows prediction of the carrier phase within short intervals. Thus, we called this scheme *partially coherent* and describe it in the next section.

Partially Coherent GNSS/INS Integration

The key idea of the newly proposed integration scheme is to combine a strapdown calculation and step detection into a new trajectory type called μ -trajectory. The base solution is given by a dead reckoning algorithm that detects user steps by analyzing the total acceleration of the IMU.

Local acceleration minima identify steps (see Figure 2), and the step length is derived from the step frequency. The heading is derived from the magnetometer and the IMU gyro. Barometer readings help to determine height changes.

The μ -trajectory is composed of

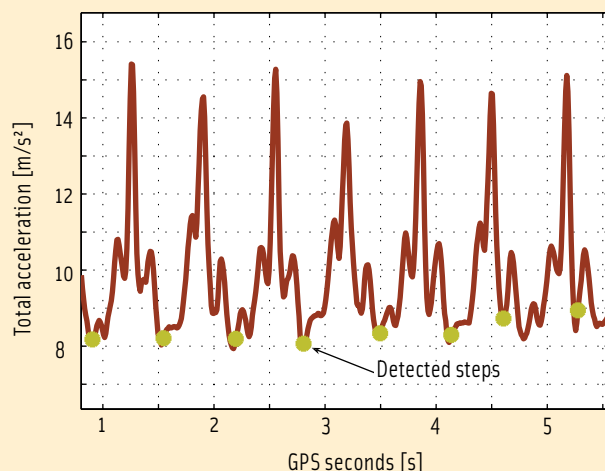


FIGURE 2 Step detection based on minima of the total acceleration

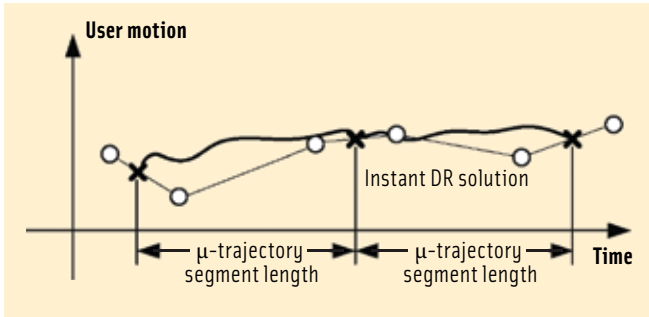


FIGURE 3 μ -trajectory (dark wavy line) fitted into the instant dead-reckoning solution (circles denote detected steps; crosses are interpolated positions). The trajectory is an estimate of the traveled path with a high time resolution.

piece-wise smooth segments. Start- and end-points of the segments are obtained by interpolating the dead reckoning solution (see **Figure 3**).

The segments are aligned with the coherent integration intervals of the GNSS signal processing. For each segment the mean strapdown acceleration and velocity is adjusted so that the strapdown trajectory connects the start and end-point.

The IMU and the GNSS antenna are mounted very close together (distance <15 centimeters), and we can therefore ignore lever-arm effects. By constraining the strapdown calculation in this way, we can estimate the *non-linear* IMU (= antenna) motion with centimeter accuracy. In other words, the μ -trajectory can be used to predict the carrier phase of single segments.

The phase of the carrier NCO is controlled by the Kalman filter during the μ -trajectory segments. Together with a data-wipe off and a stable oscillator, this algorithm allows use of coherent integration times up to several seconds. At the segments boundary, the carrier phase may change arbitrarily.

The accuracy of the μ -trajectory is demonstrated in **Figure 4**, which shows segments of the carrier phase for one GPS satellite. For each segment, the mean value, a linear term, and quadratic term have been subtracted.

The mean value corresponds to the arbitrary phase jump at the segment boundary; the linear term, to a residual Doppler frequency estimate; and the quadratic term, to the satellite orbital acceleration that is known

from the ephemeris data. A walking ($t < 177$ seconds) user is considered as well as a segment length of two seconds.

Obviously, the proposed method works perfectly for a static user ($t > 177$ seconds). It also works well for a walking user and for high elevation satel-

lites. For a walking user and lower elevations, however, the accuracy depends on the accuracy of the estimated heading. Occasionally, some intervals are affected by gross errors, e.g., incorrectly detected steps, that cause larger correlation losses in the software receiver.

Data Flow

The realization of an ultra-tight GNSS/INS system is difficult, because it requires synchronizing of various data before processing. The processing itself introduces latencies and requires suitable data buffers to accommodate these.

Figure 5 presents a block diagram of the DINGPOS scheme, including other positioning methods based on WiFi or ZigBee signal power measurements. Furthermore, the dead reckoning solution uses magnetometer and barometer data. Assistance data (ephemeris, clock, navigation data bits, start position, and

GNSS time sync.) are received from a reference receiver via a TCP/IP connection.

When the receiver starts up, it obtains a coarse time synchronization with an accuracy of around 30 milliseconds using the network time protocol (NTP) via the data link. By means of ZigBee, WiFi, or the assistance link, DINGPOS gets an approximate start position and then acquires GNSS signals via a long coherent integration. Tracking begins using *independent* receiver channels.

At the outset, the GNSS NCOs use only the μ -trajectory velocity to adjust the NCO rate values (= *tight coupling*). The integration Kalman filter (IKF) updates its error state vector with GNSS code pseudoranges and WiFi/ZigBee positions and provides position corrections and accuracy values to the μ -trajectory generator.

If the accuracy of the μ -trajectory and the clock error falls below a threshold value (e.g., 50 meters for GPS C/A code), then the system switches into *vector tracking* (= *ultra-tight coupling*). Suitable state machines control the transition between tight/ultra-tight coupling and between tracking and acquisition of GNSS signals.

To leverage the synchronization demands, we subdivided the data processing in **Figure 5** into two main lines:

- *Real-time processing*: instant dead reckoning for μ -trajectory generation and real-time position output

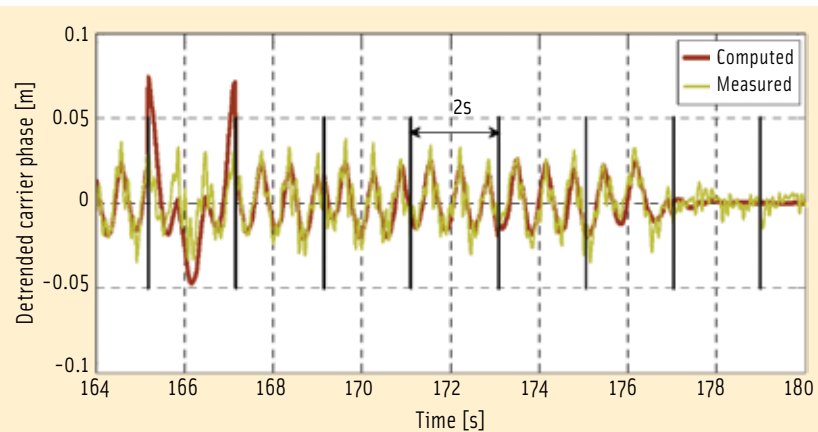


FIGURE 4 Computed (constrained strapdown) and measured GPS C/A carrier phase of PRN30 for a pedestrian using DINGPOS. Black vertical lines are the segments' boundaries.

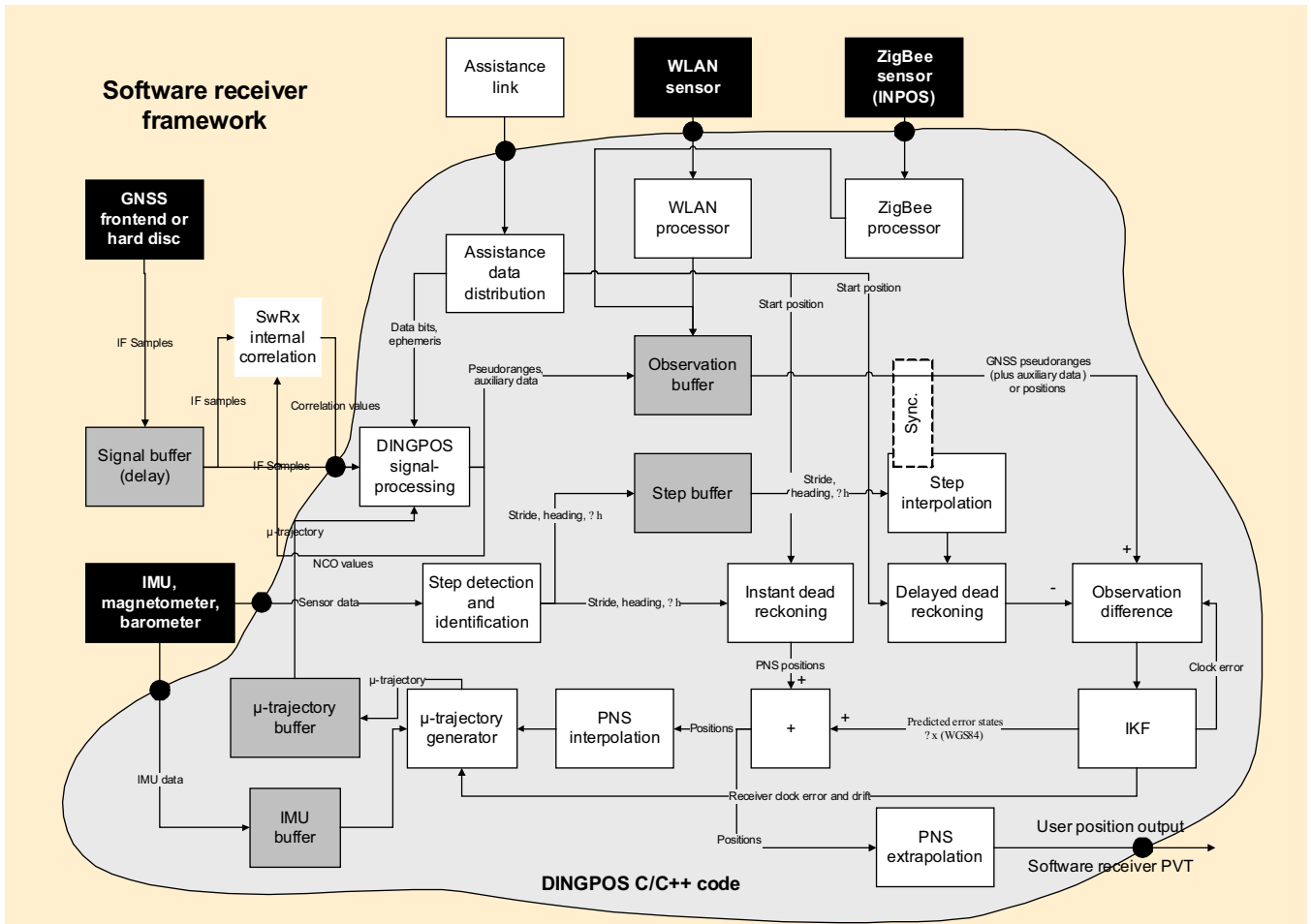


FIGURE 5 Detailed block diagram of DINGPOS GNSS/INS partially coherent, ultra-tight integration algorithm. PNS = pedestrian navigation system; IKF = integration Kalman filter. Black boxes are external sensors, gray boxes are data buffers, and circles are API interfaces.

- **Delayed processing:** delayed dead reckoning with Kalman filter error state estimation.

The delayed process collects all measurements and estimates the position error and clock error, which are extrapolated and applied to the real-time processing. The delayed processing waits until all data arrives.

The extrapolation of the state from the delayed processing to the real-time epoch can be done precisely, because the residual user dynamics (i.e., the dynamics not captured by the dead reckoning) is quite low.

Processing of data (e.g., signal correlation to convert IF samples into pseudoranges) shifts the data in the “real-time” axis but leaves the “data-time” unchanged. Step detection works almost instantly.

GNSS Signal Processing

The partially coherent GNSS/INS scheme requires modification of the well-known GNSS signal correlation formula according to

$$C = \sum_{\mu} s_{sat}(t_{\mu}) \underbrace{c(t_{\mu} - \tau(t_{\mu})) d(t_{\mu} - \tau(t_{\mu}))}_{= \text{Reference Signal}} \exp\{-i\omega t_{\mu}\} \exp\{i\Delta\varphi(t_{\mu})\} \text{ with } t_{\mu} = t_{NTP} + \frac{\mu}{f_s} \quad (1)$$

where t_{μ} denotes the internal receiver time for the received IF signal sample with index f_s .

The symbol t_{NTP} denotes the start epoch derived from querying a time server. C denotes a generic coherent correlation output (during acquisition or tracking); $s_{sat}(t_{\mu})$, the received signal samples; $c(t_{\mu} - \tau(t_{\mu}))$, the internal PRN code replica samples including the (C)BOC/BPSK modulation; $d(t_{\mu} - \tau(t_{\mu}))$, the navigation message samples; and ω , an estimation of the constant Doppler frequency.

The innovative term is represented by the predicted carrier phase $\Delta\varphi(t_{\mu})$ that is used to cancel non-linear carrier phase variations during the correlation process. This term is absent for short coherent integration times. Note that, due to the long coherent integration time, the signal delay τ becomes itself a function of the time t_{μ} .

The predicted carrier phase should match the true carrier phase $\Delta\varphi_{true}(t_{\mu})$ of the received signal as closely as possible. Deviations from the true carrier phase cause correlation losses, expressed as

$$L_{NL} = \left| \frac{1}{T_{coh}} \int_{t=t_0}^{t=t_0+T_{coh}} \exp \left\{ i \left(\Delta \varphi(t_\mu) - \Delta \varphi_{true}(t_\mu) - \omega_0 t_\mu - \varphi_0 \right) \right\} dt \right| \quad (2)$$

with

$$\omega_0, \varphi_0 = \arg \min_{\omega_0, \varphi_0} \int_{t=t_0}^{t=t_0+T_{coh}} \left(\Delta \varphi(t_\mu) - \Delta \varphi_{true}(t_\mu) - \omega_0 t_\mu - \varphi_0 \right)^2 dt \quad (3)$$

The latter equation includes an estimation of the Doppler frequency ω_0 being generated during acquisition as well as tracking.

In order to generate the previously mentioned reference signal that includes the predicted carrier phase $\Delta \varphi(t_\mu)$, the DINGPOS receiver makes available for signal correlation — in addition to the received IF signal samples $s_{sat}(t_\mu)$ — the following information:

- estimated μ -trajectory (position and velocity) plus estimation of user clock error and drift delivered from the μ -trajectory buffer
- satellite trajectory (position and velocity), satellite clock error, and navigation data bits for each satellite in view delivered from an assistance data distribution.

Acquisition

Based on the information about the start time of the received signal sample vector and the estimated distance between the considered satellite and the user, a start spreading code phase $\rho_{st,j}$ for the reference signal is calculated (the start carrier phase is set to zero) for acquisition.

As shown in the following equations, the course of the spreading code and carrier phase is incrementally calculated over the integration interval based on the relative velocity $v_{j,l}$ between the satellite j and the user in combination with the assumed user clock drift.

$$\rho_{j,\mu} = \left[\rho_{st,j} + \sum_{l=1}^{\mu} \Delta \rho_{j,l} \right] \bmod L_{Code} [\text{chips}] \quad \text{with } \Delta \rho_{j,l} = \left(f_{code} / f_s \right) \cdot \left[l + \hat{\delta}_{rec} + \delta_{Dopp,l} + \frac{v_{j,l}}{c} \right] \quad (4)$$

$$\Delta \varphi_{j,\mu} = \left[0 + \sum_{l=1}^{\mu} \Delta \phi_{j,l} \right] \bmod 2\pi \quad \text{with } \Delta \phi_{j,l} = 2\pi \left(f_{carrier} / f_s \right) \cdot \left[\hat{\delta}_{rec} + \delta_{Dopp,l} + \frac{v_{j,l}}{c} \right] \quad (5)$$

where the signal sampling rate is represented by f_s ; L_{code} and f_{code} denote the length of the spreading code and its transmission rate, respectively.

The assumed relative receiver clock drift is given by $\hat{\delta}_{rec}$, whereas $\delta_{Dopp,l}$ denotes the l 'th candidate of the assumed Doppler frequency grid that has to be scanned, mostly due to the uncertainty about the receiver clock drift. Taking into account the data bits d and converting the spreading code phase $\rho_{j,l}$

into the spreading codeword amplitude a , one subsequently can generate the baseband replica signal to finally obtain signal correlation (1).

For acquisition, the receiver correlates the received and reference signals by applying a discrete Fourier transformation (DFT) and its inverse. Non-coherent combination of coherent correlation results is applied, if necessary, to improve performance. After the correlation values C of (1) are calculated for all Doppler frequency candidates, the maximum C is determined within the assumed timing and Doppler frequency uncertainty interval.

In order to control the pair of false alarm and detection rate, the maximum peak is only accepted if the ratio between the maximum and the average correlation value in the uncertainty interval exceeds a chosen threshold.

Tracking

While tracking a satellite signal, internal optimized routines of the software receiver are used to generate the punctual and early-late correlation values for every spreading codeword. The “internal correlation” block (refer to Figure 5) receives an actual value of the code and carrier phase rate for each PRN code sequence (e.g. every 1-ms for GPS the C/A-code). Both rates are determined based on the actual relative velocity between user and satellite (derived from the corresponding μ -trajectory data) and clock drifts.

In addition, the NCO code phase is set at the start of a long coherent integration interval in case of vector tracking. Its calculation is based on the corresponding pseudorange that is determined from the satellite and user μ -trajectory data, clock errors, and the modeling of the ionospheric and tropospheric error. Thus, the internal code phase can “jump” at coherent integration interval borders.

The partial correlation results for each codeword in the integration interval are held in memory and are coherently combined to obtain the total result. The availability of the partial correlation results creates the opportunity to combine them alternatively, assuming an additional frequency offset ω , the size of which is determined by the accuracy of the clock drift estimation. Consequently, one can generate punctual correlation results as a function of an assumed residual frequency offset grid.

Finally, one selects that punctual correlation value with the largest magnitude and assumes the corresponding frequency offset as the actual frequency discriminator value (= *maximum likelihood Doppler estimation*). This allows DINGPOS to maintain long coherent accumulation intervals, although the clock drift changes might be larger than the inverse of the coherent integration time (such changes would spoil a standard carrier tracking loop).

At the end of an integration interval, the receiver calculates updated pseudoranges that combine the pseudoranges at the start of the interval, the change of the geometric distance (based on user and satellite trajectory) during the interval, clock drifts, and the code and frequency phase discriminator outputs determined at the end of the interval. The updated

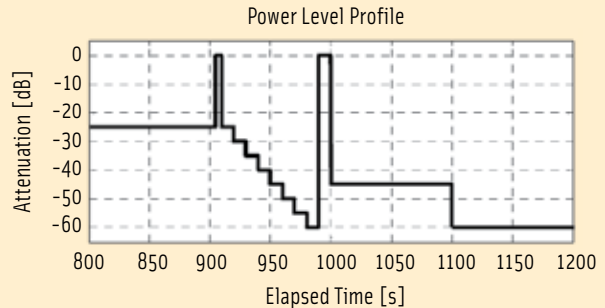
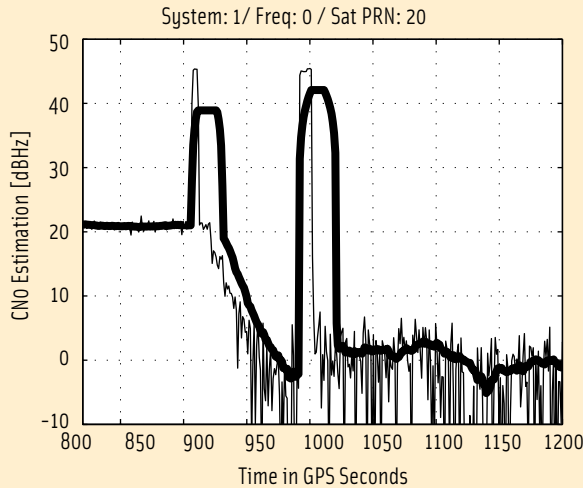


FIGURE 6 Left: Estimated C/N_0 during tracking of an E1B+C signal (bold line is a 20-second running average of the thin line); right: nominal signal attenuation (0 dB - 46.5 dBHz)

pseudoranges are provided to the observation buffer (refer to Figure 5) for further processing.

Test Results

We will present the results of two tests of the DINGPOS prototype. The satellite signals were generated by an RF level GNSS signal simulator which is connected to the software receiver. The GNSS signal simulator is synchronized to a simulation of the dead reckoning, WiFi, ZigBee, and μ -trajectory subsystems.

The test design assumes that the user walks along a rectangle. The simulated trajectory is based on RTK data derived from an actual pedestrian excursion. The μ -trajectory subsystem generates trajectory segments with a length of one second.

The first test shows an example of the estimated carrier-to-noise ratio (C/N_0) during tracking of a Galileo E1B+C signal (Figure 6) together with the power profile that is applied during signal generation. We used a coherent integration time of one second without non-coherent combinations.

The receiver starts with independent channel tracking and after 825 seconds switches to vector tracking using six satellites. The averaged C/N_0 (bold line in Figure 6) also nicely demonstrates the difference of a nominal C/N_0 of 1.5 dBHz ($t = 1000 - 1100$ s) and, if no signal is present, ($t = 1100 - 1200$ s). This is one method to verify that the system is able to track GNSS signals at 1.5 dBHz over 100 seconds. Further tests will indicate the ultimate sensitivity of the system.

The second test result shows the obtained squared correlation values at the acquisition of a Galileo E1B+C (PRN1) signal with a $C/N_0 = 3$ dBHz. The peak search spans 24 millisecond in the time domain and 8 hertz in the frequency domain. A coherent integration interval of one second with 20 non-coherent combinations is applied. Figure 7 clearly shows the true correlation peak at zero delay and a Doppler frequency offset of approximately four hertz, verifying that the quality of the μ -trajectory segments is sufficient to support a coherent integration time of one second.

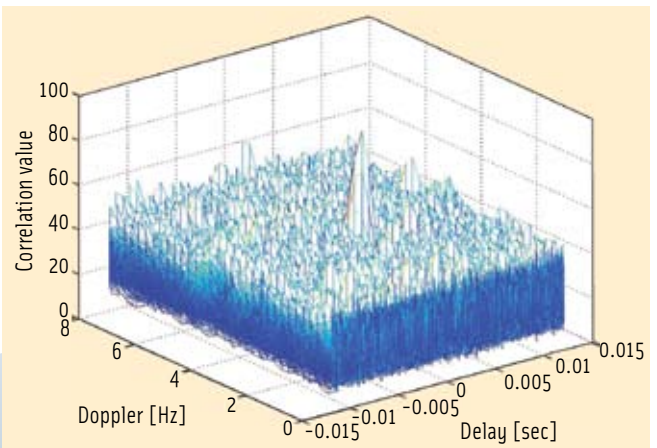


FIGURE 7 Acquisition correlation values vs. Doppler bins and uncertainty interval (Galileo E1B+C, Sat PRN1, 3 dBHz)

Benefits of Long Coherent Integration

Coherent integration provides a number of advantages compared to non-coherent integration. These benefits shall be outlined in the following sub-sections.

Multipath Mitigation in the Doppler Domain. The correlation process itself suppresses multipath signals if the multipath Doppler frequency differs from the line-of-sight Doppler frequency. This phenomenon is related to synthetic aperture signal processing and in more elementary terms is called pre-correlation suppression.

A multipath signal is suppressed by

$$L_{pre}(f_D) = \text{sinc}(\pi f_D T_{coh}) \quad (6)$$

where f_D is the Doppler difference of the line-of-sight signal to the multipath signal.

For an omnidirectional antenna and a user moving with a speed v , the multipath probability expressed as a function of the Doppler difference is given by the Jakes density:

$$P(f_D) = \begin{cases} \frac{1}{\pi f_{Dmax} \sqrt{1 - \left(\frac{f_D}{f_{Dmax}}\right)^2}} & \text{for } |f_D| < |f_{Dmax}| \\ 0 & \text{otherwise} \end{cases} \quad (7)$$

where the maximum possible Doppler frequency f_{Dmax} is

$$f_{Dmax} = f_0 \frac{2v}{c} \quad (8)$$

Figure 8 shows the Jakes PSD ($v = 1$ m/s) and the product $L_{pre}(f_d)P(f_d)$. For coherent integration times larger than 20 milliseconds, multipath is mitigated.

Cross-Correlation Protection by Data Wipe-Off. When we want to track a weak indoor signal, we face the problem that cross-correlation peaks of a strong signal (coming through a window, for example) with the weak signal replica are occasionally larger than the desired auto-correlation peak.

The PRN codes themselves provide a certain level of cross-correlation protection. This protection is enhanced when integrating over intervals longer than a data bit, assuming that the data bits from the two satellites differ from each other. Mathematically, the normalized cross-correlation is expressed as

$$R(\tau, \omega, d) = \frac{\left| \sum_{\mu} c_w(t_{\mu} - \tau) d_w(t_{\mu} - \tau) c_s(t_{\mu}) d_s(t_{\mu}) \exp\{i\omega t_{\mu}\} \right|}{\sum_{\mu} c_w(t_{\mu} - \tau)^2 d_w(t_{\mu} - \tau)^2} \quad (9)$$

where the indices s and w refer to the strong and weak signal. The cross-correlation depends on the relative code phase τ and Doppler ω of the two signals as well as on the given data bit configuration d .

For independent channel tracking, the channel of the weak signal may lock onto a cross-correlation peak. The protection (expressed as signal power difference) is

$$P_{Xcorr}(d) = \max_{\tau, \omega} R(\tau, \omega, d) \quad (10)$$

Averaging over all data bit configurations, the cross-correlation protection is obtained by

$$P_{Xcorr} = 20 \log_{10} \langle P_{Xcorr}(d) \rangle_d \quad (11)$$

Assuming the data bits are independent binary $\{+1, -1\}$ and uniformly distributed random variables, an admissible code phase shift of $[0 \dots 1023]$ chips and an admissible Doppler difference from -5 kHz to $+5$ kHz in steps of 500 hertz yields the numerical values listed in Table 1 for the GPS C/A code signal. Data bit transitions are assumed to be non-aligned and a number of 500 data bit configurations was considered.

Cross-Correlation Protection by Vector-Tracking. When a receiver is in the vector-tracking mode, which makes use of inter-satellite path correlation, it cannot lock onto a signal cross-correlation peak because it is virtually impossible that the cross-correlation peak follows the desired auto-correlation peak. Vector tracking (with the help of the other receiver channels or the IMU) pushes the channel away from the cross-cor-

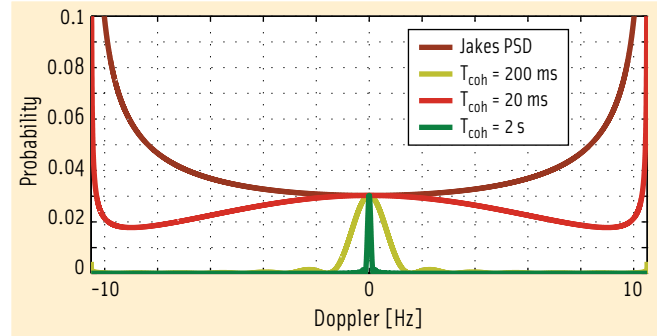


FIGURE 8 (Effective) multipath probability for various correlation times

relation peak.

In contrast, an independent channel may lock onto the cross-correlation peak. Overall, the cross-correlation protection is enhanced by vector tracking, because

the cross-correlation effect on signal tracking changes its nature. The cross-correlation *only* acts as an additional noise to weak signal tracking with a noise power of

$$P_{Xcorr} = 10 \log_{10} \langle R(\tau, \omega, d) \rangle_{d, \tau, \omega}^2 \quad (12)$$

Examples of protection values are listed in Table 1. A value of 0 decibel (in the vector tracking column) means that the cross-correlation noise power is identical to the auto-correlation power. Overall, we find that in vector tracking and with a two-second coherent integration time, cross-correlation is perfectly mitigated.

Reduced Squaring Loss. It is well known that the accuracy σ_{obs} of a code pseudorange measurement (or a Doppler measurement) follows the generic formula

$$\sigma_{obs}^2 : \alpha \frac{B}{C/N_0} \left(1 + \frac{\beta}{T_{coh} C/N_0} \right) \quad (13)$$

Here B is the tracking loop bandwidth, and α is a suitable constant. For low C/N_0 values, the squaring loss (the term in the parentheses) strongly increases. The squaring loss is partially mitigated by a longer coherent integration time. Furthermore, the squaring loss also diminishes the acquisition sensitivity.

Other Building Blocks

Even the most sophisticated GNSS signal processing will come to its end in a severe indoor environment. To continue the positioning service, DINGPOS receivers use WiFi and ZigBee sensors. Furthermore, the receiver oscillator and the assistance data link is of utmost importance as the time dimension cannot be aided by the IMU. Map-matching is not considered in this project but is a very suitable tool to stabilize the user trajectory.

Receiver Oscillator. As shown in equation (2), the receiver clock error needs to be linear during the coherent integration

| Coherent integration time | Independent channel protection (11) | Vector tracking protection (12) |
|---------------------------|-------------------------------------|---------------------------------|
| 20 ms | -21.1 dB | -38.7 dB |
| 200 ms | -27.1 dB | -54.0 dB |
| 2 s | -32.5 dB | -61.3 dB |

TABLE 1. PRN1/2 GPS C/A cross-correlation protection in independent channel mode and vector tracking mode.

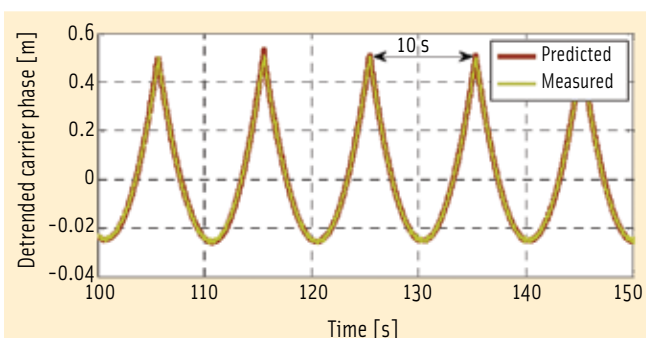


FIGURE 9 Segments of 10-second duration of the predicted and the measured GPS C/A carrier phase (PRN29) for a static position.

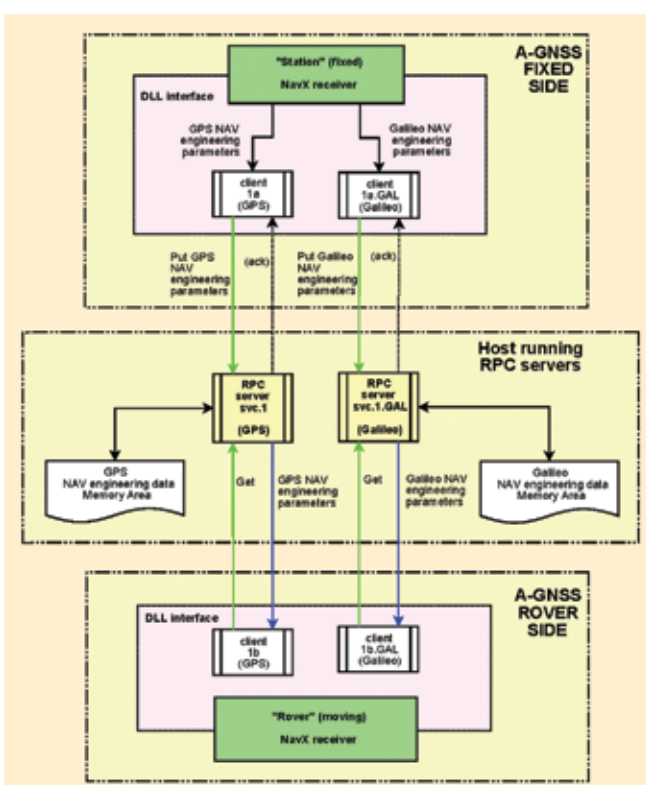


FIGURE 10 DINGPOS solution for exchanging NAV message engineering information

prompt correlator. The true carrier phase is compared against a prediction based on previous IKF estimate of the clock drift. Figure 9 shows the segment-wise detrended values of the true and predicted carrier phases.

The parabolic shape of the individual segments is caused by the satellite acceleration during the coherent integration interval of 10 seconds. We found that the OCXO is quite stable and 10-second correlation losses are well below one decibel. Our experience is in concordance with the conjecture in the paper by G. López-Risueño (see Additional Resources) that (14) is a quite conservative bound.

Assistance Data Link. DINGPOS signal processing relies on the availability of satellite ephemeris and clock information as well as on the broadcast navigation data bits. These data are transferred over a TCP/IP-based link. The rover internally delays signal processing by several seconds to allow a certain delay in the assistance data transfer. Such a delay is eventually caused by the use of wireless communication means — by nature prone to discontinuity — due to a slow connection or even an interruption of the transmission link.

The assisted-GNSS (A-GNSS) solution relies upon a remote procedure call (RPC) client-server architecture, aiming to exchange data between indoor (fixed) and outdoor (roving) platforms, strongly mitigating uncertainty on wireless link continuity. RPC provides a good compromise between complexity, efficiency, real time operation, and robustness, at the price of a very limited overhead on the size of exchanged IP packets.

Both the indoor and the outdoor operating software receivers are supplemented with a custom RPC application layer and RPC client functions, through DLL components loaded into the receiver. Figure 10 depicts transfer of GPS/Galileo navigation information encoded in an engineering format. Note that RPC servers can be, in principle, activated on any host within the DINGPOS wireless LAN.

The software receiver's interface DLL implementation is such that in case of a wireless communication signal loss, RPC clients attempt to autonomously restore their connection with servers. Queues allow the system to mitigate asynchronous aspects in the operation between two sides (fixed, rover) and any eventual temporary lack of digital communication exchange capability. Critical information is never lost or corrupted and can be retrieved at later time instants, as soon as a new, successful digital connection is established.

WiFi and ZigBee Sensor. Because the positioning error of dead reckoning systems grows with time and distance traveled and GNSS is often severely degraded indoors, other means of position updates have to be found for those scenarios. WiFi can be used to provide proximity positions in such environments. Nowadays, in most buildings WiFi access points are installed that can be used as the necessary infrastructure.

WiFi can be used for positioning, measuring the received signal strength (RSS). Ranging of several access points (APs) is not feasible today, because precise time synchronization of WiFi APs has not been implemented so far. This may change in the future.

time. Oscillator jitter or drift changes may otherwise corrupt the correlation results. A conservative bound

$$T_{coh} \sigma_A (T_{coh}) f_{RF} = 0.5 \quad (14)$$

of the oscillator Allan variance at $T_{coh} = 10$ seconds requires it to be much smaller than 3.2×10^{-11} [9] to achieve a coherent integration time of 10 seconds. The specification of the oven-controlled crystal oscillator (OCXO) GNSS front-end used in the DINGPOS provides a typical Allan variance at 10 seconds of 10^{-11} .

We can explicitly verify correlation losses due to the OCXO jitter by measuring the true carrier phase $\Delta\phi_{true}(t_\mu)$ for a given GPS satellite at high signal-to-noise values. The test setup requires a static user position. The true carrier phase is computed as the unwrapped argument of the complex valued



FIGURE 11 ZigBee-based positioning system

The WiFi interface card of the DINGPOS notebook computer is used to determine the access point that is nearest to a user. The software receiver scans the visibility of all access points and provides their signal strength (RSSI, received signal strength indicator) in an interval of two to three seconds.

Based on the MAC (media access control) addresses and SSIDs (Service Set Identifiers) of the network nodes, the access points are uniquely identified and mapped to their known coordinates in WGS84. Proximity is determined by a system of several rules with the main parameter being the RSS of individual APs. To establish proximity to an individual AP, its RSS must exceed a predefined threshold. By adjusting this threshold, the detection range can be adjusted.

Secondly, a significant RSS difference to neighboring APs must be measured, with signal strength differences usually in the range of two to four decibels. When a user is near a strong-signal AP, the measured signal strength of other strong APs decreases. This RSS fading allows the use of the derivative of the RSS values of neighboring APs to determine that the user is in the proximity of the strong-signal AP.

Another positioning option is provided by a ZigBee-based positioning system attached to the DINGPOS receiver. It consists of a wireless direct sequence spread spectrum radio module operating in the 2.4 GHz ISM band, integrated with a USB digital interface board (see Figure 11).

ZigBee positioning exploits “fingerprints of received signal strength measurements obtained during a calibration campaign. The roving ZigBee device receives wireless signals from a number of fixed RF emitters of the same type; user position is established based on received power levels from each individual source.

Positioning Results

The DINGPOS receiver prototype is currently the subject of intensive testing. Especially when using postprocessing techniques, the system clearly outperforms GPS-only high sensitivity solutions.

A typical positioning result is shown in Figure 12. It is obtained in a mixed outdoor/indoor environment. Outside the GPS C/A signal strength is around 33-52 dBHz. Inside the building it falls below 10 dBHz; only occasionally 1-2 satellites reach higher power levels. Due to the UTC scheme and the stable oscillator, the system is able to track all GPS signals continuously.

Furthermore, the system mitigates multipath (see mark in Fig. 12, that occurs before entering the building) when a 2-second coherent integration time is used instead of 57 non-coherent summations of 35-millisecond coherent intervals. Note: the rather odd value of 35 milliseconds is due to a technical limitation during data recording, but 35 milliseconds is considered to be representative for the typical value of 20 milliseconds.

Conclusions

So far, the system clearly demonstrated the ability to integrate coherently up to two seconds (dynamic) or up to 10 seconds (static) in the tracking mode. Signal acquisition can reach up to one-second coherent integration time. All values might increase in future. The simulations carried out with the signal simulator nicely verified the expected performance with the GPS/Galileo/GATE signals on L1=E1 and L5=E5a.

Of special importance is the use of the L5 signals. Switching from a BPSK(1) signal to a BPSK(10) signal

roughly corresponds to an equivalent C/N_0 increase of between 20 decibels (no squaring loss) and 40 decibels (with squaring loss) in terms of equivalent thermal noise ranging errors.

The test with a real GPS C/A-code signal demonstrated that the system is able to track signals better than a state-of-the-art chip set. Furthermore, gross pseudorange errors (caused by cross-correlations or as loss-of-lock precursors) were virtually absent with vector tracking switched on and a long coherent integration time. Multipath is successfully mitigated in the Doppler domain.

Acknowledgment

The presented work was performed in the ESA funded contract: DINGPOS, ESTEC Ctr. No. 20834.

Manufacturers

The software receiver used in the DINGPOS project is the NavX-NSR V2.0 and the signal simulator is the NavX-NCS, both from IFEN GmbH, Poing, Germany. The system incorporates the MTi inertial measurement unit with magnetometer from Xsens, B.V., Enschede, The Netherlands, the NAVport 2 front-end with integrated barometer an OCXO from IFEN, and the Zephyr 2 antenna from Trimble, Sunnyvale, California, USA. The WiFi positioning engine soft-



FIGURE 12 Real GPS C/A positioning results (thin black line = true trajectory, thick black line = dead reckoning, green line = ultra-tight coupled (UTC) GNSS/INS solution with two-second coherent integration time, red line = UTC solution with 35 millisecond coherent integration time and 57 non-coherent integrations)

ware is from **University FAF Munich**, Germany. The INPOS ZigBee positioning engine incorporates the IRIS Mote wireless DSSS radio module and an MIB520 USB digital interface board from **Crossbow Technology**, San Jose, California, USA, and software from **Telespazio S.p.A.**, Rome, Italy. The A-GNSS data distribution software is also from Telespazio.

Additional Resources

- [1] Abbott, A. S., and W. E. Lillo, inventors. Global positioning systems and inertial measuring unit ultratight coupling method. USA. no. 6516021, 2003
- [2] Landis, D., and T. Thorvaldsen, B. Fink, P. Sherman, and S. Holmes, "A Deep Integration Estimator for Urban Ground Navigation," *PLANS 2006, IEEE/ION Position, Location and Navigation Symposium*, pp. 927-932, San Diego, California, USA
- [3] López-Risueno, G., and D. Jiménez-Baños, F. González-Martínez, P. Waller, and M. Colina-Fatjo, "User Clock Impact On High Sensitivity GNSS Receivers," *Proceedings ENC-GNSS 2008*, Toulouse, France
- [4] Niedermeier, H., and G. Ameres, T. Pany, B. Eissfeller, J. Winkel, and G. Lopez-Risueno, "Reproduction of User Motion and GNSS Signal Phase Signatures Using MEMS INS and a Pedestrian Navigation System for HS-GNSS Applications," *Proceedings of the 4th ESA Workshop on Satellite Navigation User Equipment Technologies, NAVITEC*, Noordwijk, The Netherlands, 2008
- [5] Petovello, M. G., and C. O'Driscoll and G. Lachapelle, "Weak Signal Carrier Tracking Using Extended Coherent Integration With an Ultra-Tight GNSS/IMU Receiver," *Proceedings ENC-GNSS 2008*, Toulouse, France
- [6] Soloviev, A., and F. van Graas, M. Miller, M., and S. Gunawardena, "Synthetic Aperture GPS Signal Processing, Concept and Feasibility Demonstration," *Inside GNSS*, vol. 4, no. 3 (May/June 2009), pp. 37-46b (extended version available on-line at <<http://www.insidegnss.com/node/1453>>)
- [7] So, H., and T. Lee, S. Jeon, J. Kim, C. Kee, and M.-B. Heo, "Use of a Vector-based Tracking Loop Receiver for Solving the Near-Far Problem in a Pseudolite Navigation System," *Proceedings ION GNSS-2009*, Savannah
- [8] Winkel, J., *Modeling and Simulating GNSS Signal Structures and Receivers*, University of Federal Armed Forces Munich, Werner-Heisenberg-Weg 39, D-85577 Neubiberg, <<http://www.unibw.de/unibib/digibib/ediss/bauv>>, 2003
- [9] Won, J.-H., and D. Dötterböck and B. Eissfeller,

"Performance Comparison of Different Forms of Kalman Filter Approach for a Vector-Based GNSS Signal Tracking Loop," *Proceedings of ION GNSS 2009*, Savannah, Georgia, USA

Authors



Dr. Thomas Pany works for IFEN GmbH as a senior research engineer in the GNSS receiver department. For four years he was assistant professor (C1) at the University FAF Munich and for four years research associate at the Space Research Institute of the Austrian Academy of Science. His research interests include GNSS receivers, GNSS/INS integration, signal processing, and GNSS science.



Dr. Jón Winkel is head of receiver technology at IFEN GmbH since 2001. He studied physics at the universities in Hamburg and Regensburg. He received a Ph.D. (Dr.-Ing.) from the University of the Federal Armed Forces in Munich with a focus on GNSS modeling and simulations.



Bernhard Riedl received his diploma in electrical engineering and information technology from the Technical University of Munich. Since 1994 he has been concerned with research in the field of real-time GNSS applications at the University FAF Munich. In 2006 he joined IFEN GmbH, where he is currently working as product development manager.



Dr. Thomas Würz co-founded AUDENS ACT GmbH in 1998 and works as managing director and senior consultant. His expertise comprises satellite system design and corresponding signal processing for communication and navigation systems, such as analysis and modeling of (mobile) satellite channels, signal structures and corresponding receiver design.



Dr. Robert Schweikert co-founded for AUDENS ACT GmbH in 1998 and works as managing director and senior consultant. His expertise comprises satellite system design and corresponding signal processing for communica-

tion and navigation systems, such as analysis and modeling of (mobile) satellite channels, signal structures, and corresponding receiver design.



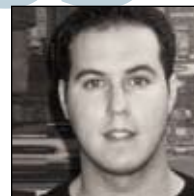
Herbert Niedermeier is a mechanical engineer in the field of aeronautical engineering and research associate at the Institute of Geodesy and Navigation at the University FAF Munich. He is working on sensor fusion for different applications, e.g., pedestrian or vehicle navigation, with an emphasis on airborne gravimetry. Current research is focused on inertial navigation and sensor integration, particularly for pedestrian and vehicle navigation.



Stefano Lagrasta has a master's degree in electronics engineering and leads the Navigation Systems and Services engineering unit at Telespazio, with former experience on design and implementation of satellite attitude control and ground flight dynamics systems.



Dr. Gustavo López-Risueno has a Ph.D. and an M. Sc. in telecommunications engineering, from the Universidad Politécnica de Madrid, Spain. He has held several positions in academia, ESA and NC3A (NATO). Currently, he is a radionavigation systems engineer at ESA/ESTEC working mainly on signal processing for GNSS receivers and monitoring.



David Jiménez-Baños has M. Sc. degrees in telecommunications engineering and information and communication technologies from the Universitat Politècnica de Catalunya. Since 2006 he has been working at the Radio Navigation Systems and Techniques section of ESA/ESTEC, The Netherlands. His main areas of work have been on GNSS signal processing for indoor applications, SBAS systems, and GNSS simulation tools for receiver performance evaluation, and, more recently, GNSS signal processing techniques for AOCS applications in GEO and higher orbits and interference modelling and mitigation techniques. 